A Two-stage Image Segmentation Method Using Euler's Elastica Regularized Mumford-Shah Model

Yuping Duan
Neural & Biomedical Technology Department
Institute for Infocomm Research, Singapore, 138632
Email: duany@i2r.a-star.edu.sg

Huibin Chang
Department of Mathematical Sciences
Tianjin Normal University, P.R. China, 300387
Email: changhuibin@gmail.com

Weimin Huang, Jiayin Zhou
Neural & Biomedical Technology Department
Institute for Infocomm Research, Singapore, 138632
Email: {wmhuang, jzhou}@i2r.a-star.edu.sg

Tieyong Zeng
Department of Mathematics
Hong Kong Baptist University, Hong Kong
Email: zeng@hkbu.edu.hk

***Abstract*—As one of the most important image segmentation models, the Mumford-Shah functional was developed to pursue a piecewise smooth approximation of a given image based on the regularization on the total length of curves. In this paper, we modify the Mumford-Shah model using Euler's elastica as the regularization. A two-stage segmentation method is applied the Euler's elastica regularized Mumford-Shah model. The first stage is to find a smooth solution of the variant Mumford-Shah functional based on augmented Lagrangian method while a thresholding is performed in the second stage to obtain different phases for the segmentation. The K-means clustering method is used as the technique to find the thresholds for the segmentation. For intensity inhomogeneous images, we eliminate the effect of the bias field by bias-corrected fuzzy c-means method. Experimental results show that as the regularization, Euler's elastica makes the Mumford-Shah model perform better for many kinds of images, including tubular and irregular shaped, CT Angiography (CTA) and MRI images in different noise level.**

I. Introduction

As a fundamental topic in image processing, the goal of image segmentation is to decompose the image domain into local regions. Such techniques are critical in computer aided diagnosis and computer aided treatment. For example, accurate segmentation of coronary arteries is important to quantify coronary artery stenosis.

Mumford and Shah [1] treated the given image as a function and pursued its piecewise smooth approximation, in which the boundaries are referred to the transition between adjacent patches of the approximation. Let $\Omega \in \mathbb{R}^2$ be open and bounded and Γ be a closed subset in Ω. Given an observed image $f : \Omega \to \mathbb{R}$, to find its piecewise smooth approximation g, Mumford and Shah proposed to minimize the following functional:

$$E_{MS}(g,\Gamma) = \frac{\eta}{2}\int_{\Omega}(f-g)^2dx + \frac{\mu}{2}\int_{\Omega\setminus\Gamma}|\nabla g|^2dx + |\Gamma|, \quad (1)$$

where η and μ are positive parameters and $|\Gamma|$ denotes the length of Γ. Since the Mumford-Shah functional (1) is non-convex, finding the minimizer is not straightforward and may trap in local minima.

One of the most successful relaxation of the Mumford-Shah functional was proposed by Chan and Vese [2], which seeks for an approximation of the given image with a binary piecewise constant representation through a level set formulation. Let $\omega \subset \Omega$ be an open subset, denoting $\Omega_1 = \omega$, $\Omega_2 = \Omega\setminus\omega$, Chan-Vese model can be expressed as the minimization of the following energy:

$$E_{CV}(c_1,c_2,\Gamma) = \frac{\eta}{2}\int_{\Omega_1}(f-c_1)^2 + \frac{\eta}{2}\int_{\Omega_2}(f-c_2)^2 + |\Gamma|, \quad (2)$$

where c_1, c_2 are two constants that approximate the image intensity in Ω_1 and Ω_2, respectively. The two-region segmentation model (2) was extended by Vese and Chan to multiple regions in [3] using a multiple level set formulation for more general segmentation problems. Due to the assumption that images consist of statistically homogeneous regions, these models are usually called piecewise constant (PC) models. To overcome the rigorous restriction of PC models, some attempts aim to minimize the Mumford-Shah functional in piecewise smooth (PS) formulations [3], [4]. Similarly, the Mumford-Shah functional is reformulated by employing level set functions and elliptic type equations are required to be solved. Therefore, both models are computational expensive and require a very good initialization to guarantee global minima. Recently, a two-stage Mumford-Shah (TSMS) model was proposed [5], which separates the segmentation task of minimizing the functional (1) into two stages: the first stage of finding a smooth solution to a convex variant of the Mumford-Shah functional and the second stage of thresholding the solution into different phases for segmentation. There are good characteristics in both stages to make the two stage segmentation framework user friendly, i.e.,

① The convex variant Mumford-Shah functional in the first stage has the global minimizer g, which can be easily and quickly computed by standard optimization techniques, such as the split-Bregman algorithm and the Chambolle's dual method;

② The thresholding in the second phase is done by either K-means method or user specified threshold(s), which can be solved quickly;

③ There is no need to 1) specify the number of segments K ($K \geq 2$) in the first stage and 2) recompute

1051-4651/14 $31.00 © 2014 IEEE
DOI 10.1109/ICPR.2014.30

IEEE computer society

g if the thresholds are changed to reveal different segmentation features.

In fact, accurate segmentation of medical images still faces difficulties because of the presence of small foreground structures and the existence of noises. Unlike the Mumford-Shah functional (1), in which the total length of curves serves as the regularization of the boundaries, we propose a novel Mumford-Shah model by employing Euler's elastica as the regularization. Euler's elastica was first introduced by Mumford [6] as a curve model

$$E(\Gamma) = \int_\Gamma (a + b\kappa^2) ds = a\text{Length}(\Gamma) + b\int_\Gamma \kappa^2 ds, \quad (3)$$

where κ is the curvature, s is arc length and a, b are tunable positive weights. In (3), if $a = 0$, $E(\Gamma)$ measures the total curvature of the curve while if $b = 0$, $E(\Gamma)$ measures the total length of the curve. Therefore, Euler's elastica minimizes the total curvature of each level line in the image.

In [7], the authors used Euler's elastica as the regularization in the Chan-Vese model (2) for binary image segmentation. In this work, we directly apply Euler's elastica to the Mumford-Shah functional (1) by taking the advantage of properties of Euler's elastics for multi-phase segmentation. As a powerful tool for image inpainting [8], [9], Euler's elastica can integrate missing or broken parts to generate complete objects. Euler's elastica was also implemented to image denoising [10], [11] to capture objects without preserving other negligible dots such as noise.

In addition, intensity inhomogeneity widely occurs in many real images of different modalities. It is often seen in medical imaging, such as MR and CT images, which is caused by limitations in imaging devices and subject-induced susceptibility effect. Such intensity inhomogeneity can lead to serious misclassifications when intensity-based segmentation models are implemented. There exist several inhomogeneity correction methods, that could be applied before the segmentation. In this paper, we apply the two-stage segmentation framework similar to [5] to our Euler's elastica regularized Mumford-Shah functional. More specifically, the proposed model has the following features

① In the first stage, we solve the Euler's elastica regularized Mumford-Shah model, which is a high order model, by making use of the augmented Lagrangian method (ALM) [12], [11];

② In the second stage, we implement the K-means clustering [13] to threshold the solution into different phases. Special attention has been paid to images with intensity inhomogeneity. We use the bias-corrected fuzzy c-means method [14] to eliminate the effect of bias field, which makes the model be able to segment the images correctly.

Similar to [5], the proposed two-stage segmentation model is flexible to the number of segments ($K \geq 2$) and free to change the value of K without recomputation of the first stage.

II. Two-stage Mumford-Shah model

We briefly introduce the TSMS model in the first place. The first stage of TSMS model is to find a smooth image g that can facilitate the segmentation. In Mumford-Shah functional (1), the boundary information of Γ, i.e., $|\Gamma|$, can be extracted using the total variation and the solution of (1) is further restricted to be a smooth function over the image domain. Therefore, the last term of (1) reduces to the total variation of g in order to keep the boundary information, and the second term of (1) reduces to the integral over the entire domain Ω assuming that $g \in W^{1,2}(\Omega)$, respectively. For the definition of Sobolev space $W^{1,2}(\Omega)$, see [15].

The variant convex Mumford-Shah proposed in [5] is given as follows

$$E_{TSMS}(g) = \frac{\eta}{2}\int_\Omega (f-g)^2 dx + \frac{\mu}{2}\int_\Omega |\nabla g|^2 dx + \int_\Omega |\nabla g| \quad (4)$$

With the solution g solved in the first stage by (4), the segmentation results are obtained by thresholding g with proper threshold(s). The thresholds are identified in [5] is automatically by K-means clustering method for arbitrary K given by users. However, simply using the K-means clustering may be not so satisfactory. It requires users to try different thresholds for better segmentation results.

III. Euler's elastica regularized Mumford-Shah model

A. Stage I: obtain the smooth solution g

Although the TSMS model works well for general images, it fails for real images with specific properties, e.g., with high noises, missing parts, intensity inhomogeneity. Therefore, we modify the Mumford-Shah model by employing Euler's elastica as the regularization and obtain the following functional:

$$\begin{aligned} E_{EEMS}(g) =& \frac{\eta}{2}\int_\Omega (f-g)^2 dx + \frac{\mu}{2}\int_\Omega |\nabla g|^2 dx \\ &+ \int_\Omega \big[a + b(\nabla \cdot \frac{\nabla g}{|\nabla g|})^2\big]|\nabla g|. \end{aligned} \quad (5)$$

The main disadvantage of such high order model is the difficulty and complexity of computation. Therefore, we convert the minimization problem (5) to the constrained optimization problem by introducing new variables into the functional as

$$\begin{aligned} &\min_{g,\mathbf{p},\mathbf{n}} \int_\Omega \big(a + b(\nabla \cdot \mathbf{n})^2\big)|\mathbf{p}| + \frac{\mu}{2}\int_\Omega |\nabla g|^2 + \frac{\eta}{2}\int_\Omega (f-g)^2 \\ &\text{s.t.} \quad \mathbf{p} = \nabla g; \quad \mathbf{n} = \frac{\mathbf{p}}{|\mathbf{p}|}. \end{aligned} \quad (6)$$

ALM has been utilized in developing the fast algorithm for Euler's elastica energy in [11]. Similarly, to avoid the difficulties in solving the Lagrangian functional of (6), a new variable $\mathbf{m}$ is introduced, which satisfies $\mathbf{m} = \mathbf{n}$ and $|\mathbf{m}| \leq 1$. Here, the use of $\boldsymbol{m}$ with $|\boldsymbol{m}| \leq 1$ is a relaxation, the same as [11]. Thus, the relationship $|\mathbf{p}| - \mathbf{m}\cdot\mathbf{p} \geq 0$ holds, a.e., in Ω. We can derive the augmented Lagrangian functional in the following form

$$\begin{aligned} &\mathcal{L}(g,\mathbf{p},\mathbf{n},\mathbf{m};\lambda_1,\boldsymbol{\lambda}_2,\boldsymbol{\lambda}_3) = \int_\Omega \big(a + b(\nabla\cdot\mathbf{n})^2\big)|\mathbf{p}| \\ &+ \frac{\mu}{2}\int_\Omega |\nabla g|^2 + \frac{\eta}{2}\int_\Omega (f-g)^2 + \int_\Omega \lambda_1(|\mathbf{p}| - \mathbf{m}\cdot\mathbf{p}) \\ &+ r_1\int_\Omega (|\mathbf{p}| - \mathbf{m}\cdot\mathbf{p}) + \int_\Omega \boldsymbol{\lambda}_2\cdot(\mathbf{p} - \nabla g) + \frac{r_2}{2}\int_\Omega (\mathbf{p}-\nabla g)^2 \\ &+ \int_\Omega \boldsymbol{\lambda}_3\cdot(\mathbf{n}-\mathbf{m}) + \frac{r_3}{2}\int_\Omega (\mathbf{n}-\mathbf{m})^2 + \delta_{\mathcal{R}}(\mathbf{m}), \end{aligned} \quad (7)$$

where r_1, r_2, r_3 are positive parameters and λ_1, $\boldsymbol{\lambda}_2$, $\boldsymbol{\lambda}_3$ are Lagrange multipliers. Moreover, the set $\mathcal{R}$ is defined as $\{\ \mathbf{m} \in \mathbf{L}^2(\Omega) \mid |\mathbf{m}| \leq 1 \ \text{ a.e. in } \Omega\ \}$, $\mathbf{L}^2(\Omega) := \{\mathbf{m} \in \mathbb{R}^2 : \int_\Omega |\mathbf{m}|^2 < \infty\}$ and $\delta_{\mathcal{R}}$ is the characteristic function defined on the set $\mathcal{R}$ as follows

$$\delta_{\mathcal{R}}(\mathbf{m}) := \begin{cases} 0, & \mathbf{m} \in \mathcal{R}, \\ +\infty, & \text{otherwise.} \end{cases}$$

We propose an alternative and iterative algorithm to solve the augmented Lagrangian functional (7) as Algorithm 1.

Algorithm 1 The proposed ALM based algorithm

Set the starting values g^1, $\boldsymbol{p}^1$, $\boldsymbol{n}^1$, $\boldsymbol{m}^1$, λ_1^1, $\boldsymbol{\lambda}_2^1$ and $\boldsymbol{\lambda}_3^1$, let $k = 1$ and start $(k+1)$-th iteration, which includes the following steps till convergence:

① Optimize g^{k+1} by fixing other variables

$$g^{k+1} := \arg\min_g \int_\Omega \frac{\eta}{2}(f-g)^2 + \frac{\mu}{2}|\nabla g|^2 + \frac{r_2}{2}(\nabla g - \boldsymbol{d}^k)^2,$$

where $\boldsymbol{d}^k = \boldsymbol{p}^k + \frac{\boldsymbol{\lambda}_2^k}{r_2}$. The optimal condition is a linear equation, which is solved by the fast Fourier transform (FFT).

② Optimize $\boldsymbol{p}^{k+1}$ by fixing other variables

$$\boldsymbol{p}^k := \arg\min_{\boldsymbol{p}} \int_\Omega c^k|\boldsymbol{p}| + \frac{r_2}{2}(\boldsymbol{p} - \boldsymbol{q}^k)^2,$$

where $c^k = a + b(\nabla \cdot \boldsymbol{n}^k)^2$ and $\boldsymbol{q}^k = \nabla g^{k+1} + \frac{r_1+\lambda_1^k}{r_2}\boldsymbol{m}^k - \frac{\boldsymbol{\lambda}_2^k}{r_2}$. There is the closed-form solution for the minimization problem.

③ Optimize $\boldsymbol{n}^{k+1}$ by fixing other variables

$$\boldsymbol{n}^{k+1} := \arg\min_{\boldsymbol{n}} \int_\Omega b(\nabla \cdot \boldsymbol{n})^2|\boldsymbol{p}^{k+1}| + \frac{r_3}{2}(\boldsymbol{n} - \boldsymbol{h}^k)^2,$$

where $\boldsymbol{h}^k = (\boldsymbol{m}^k - \frac{\boldsymbol{\lambda}_3^k}{r_3})$. By applying a frozen coefficient method, the minimization problem is solved by the FFT.

④ Optimize $\boldsymbol{m}^{k+1}$ by fixing other variables

$$\boldsymbol{m}^{k+1} := \arg\min_{\boldsymbol{m}} \int_\Omega \frac{r_3}{2}(\boldsymbol{m} - (\boldsymbol{n}^{k+1} + \frac{\boldsymbol{\lambda}_3^k}{r_3}))^2 + \delta_{\mathcal{R}}(\mathbf{m}),$$

which has the closed-form solution.

⑤ Update λ_1^{k+1}, $\boldsymbol{\lambda}_2^{k+1}$ and $\boldsymbol{\lambda}_3^{k+1}$ by

$$\lambda_1^{k+1} = \lambda_1^k + r_1(|\boldsymbol{p}^{k+1}| - \boldsymbol{m}^{k+1} \cdot \boldsymbol{p}^{k+1}),$$
$$\boldsymbol{\lambda}_2^{k+1} = \boldsymbol{\lambda}_2^k + r_2(\boldsymbol{p}^{k+1} - \nabla g^{k+1}),$$
$$\boldsymbol{\lambda}_3^{k+3} = \boldsymbol{\lambda}_3^k + r_3(\boldsymbol{n}^{k+1} - \boldsymbol{m}^{k+1}).$$

B. Stage II: determine the thresholds

In the second stage, the segmentation result is obtained by thresholding the solution g with proper thresholds. The K-means method is employed to determine the thresholds of the solution g. More specifically, for images with intensity inhomogeneity, we adopt the bias-corrected fuzzy c-means method to eliminate the effect of bias field before the K-means thresholding.

The bias-corrected fuzzy c-means models the solution g as a combination of true intensities and a bias field as follows

$$g_k = x_k + \beta_k, \qquad \forall k \in \{1, 2, \ldots, M \times N\}, \tag{8}$$

where x_k, g_k are the true and observed (smooth solution in the first stage)intensities at the k-th pixel, respectively, β_k is the bias field at the k-th pixel and $M \times N$ is the total number of pixel in the given image.

Compared to the standard fuzzy c-means (FCM) algorithm, the bias-corrected FCM compensates inhomogeneity to allow the labeling of a pixel to be influenced by the labels within its neighborhood. The neighborhood effect acts as a regularization and biases the solution towards piecewise-homogeneous labeling. The objective function for partitioning g into c clusters is given by

$$E_{BCFCM} = \sum_{i=1}^{c}\sum_{k=1}^{M\times N} u_{ik}^p \|g_k - \beta_k - v_i\|^2 + \frac{\alpha}{N_R}\sum_{i=1}^{c}\sum_{i=k}^{M\times N} u_{ik}^p\Big(\sum_{g_r \in \mathcal{N}_k} \|g_r - \beta_r - v_i\|^2\Big),$$

where $\{v_i\}_{i=1}^c$ are the prototypes of the clusters and the array $[u_{ik}] = U$ represents a partition matrix (p is a weighting exponent on each fuzzy membership), $U \in \mathcal{U}$, namely,

$$\mathcal{U}\big\{u_{ik} \in [0,1] \Big| \sum_{i=1}^{c} u_{ik} = 1, \forall k, 0 < \sum_{k=1}^{M\times N} u_{ik} < M \times N, \forall i\big\}$$

and $\mathcal{N}_k$ stands for the set of neighbors that exist within a window around x_k and N_R is the cardinality of $\mathcal{N}_k$.

The optimization problem of bias-corrected FCM is given in the following form

$$\min_{U, \{v_i\}_{i=1}^c, \{\beta_k\}_{k=1}^{M\times N}} E_{BCFCM}, \qquad \text{s.t., } U \in \mathcal{U}. \tag{9}$$

There are closed-form solutions for all the variables in (9). More details of the implementation can be found in [14]. After obtained the bias field, we eliminate the effect of intensity inhomogeneity by subtracting it from the solution g. Then, by the K-means method we separate the bias-corrected g into different segments.

IV. Numerical Experiments

In this section, we describe the application of the proposed Euler's elastica regularized Mumford-Shah model with K-means clustering (EEMS) and bias-corrected FCM (BCEEMS) on synthetic and real medical images. For all tests of bias-corrected FCM, we use the 8-neighborhood, i.e., $N_R = 8$ and set $p = 2$ and $\alpha = 1$.

A. Comparisons with the TSMS model

Example 1: Incomplete letters 'UCLA'. To illustrate the advantage of Euler's elastica in integrating missing or broken parts, we apply the EEMS model to an image with incomplete letters "UCLA", as shown in Fig. 1 (a). Even though the incomplete letters can be easily recognized by human perception, the TSMS model, which is based on total variation, fails to capture

TABLE I. PRECISION AND SENSITIVITY OF NOISY IMAGE SEGMENTATION.

	Fig.3 (b)		Fig.3 (f)	
	PRE	SEN	PRE	SEN
TSMS	0.9422	0.9881	0.9925	0.9795
EEMS	0.9775	0.9881	0.9922	0.9944

the missing parts. By comparing our result with the result of TSMS model, as given in Fig. 1 (b)-(g), we observe that our method works better at connecting the missing information in the given images.

(a) Given image

(b) TSMS solution g (c) TSMS K-means (d) TSMS contour

(e) Our solution g (f) EEMS (g) EEMS contour

Fig. 1. Incomplete letters 'UCLA'. The parameters for the model (5) read $a = 10^{-2}$, $b = 15.0$, $\mu = 1.0$, $\eta = 0.5$ while the parameters for ALM are chosen as $r_1 = 2.0$, $r_2 = 10.0$, $r_3 = 1.0$.

Example 2: Hand phantom image. The experiment in Fig. 2 validates that Euler's elastica can help to achieve sub-pixel segmentation accuracy. As demonstrated in Fig. 2 (e) and (f), the EEMS model is able to identify the narrow gaps between the two middle fingers, which stick together as the TSMS model shown in Fig. 2 (b) and (c). The final contour of the EEMS model in Fig. 2 (g) accurately reflects the true shape of the hand phantom.

Example 3: Noisy image segmentation. We test the segmentation models, i.e., TSMS and EEMS on two synthetic images shown in Fig. 3. We add Gaussian white noise of mean 0 and variance 0.5 to both test images as shown in Fig. 3 (b) and (f), respectively. Based on the K-means clustering, we obtain the segmentation results of both the TSMS model and EEMS model, which are displayed in Fig. 3. We tabulate the precision and recall of the two experiments in Table I. Here, precision (PRE) is defined as the fraction of the true positive pixels to the segmented results, while sensitivity (SEN) is the fraction of the true positive pixels to the ground truth of the foreground. With the same sensitivity as the TSMS model, the EEMS model increases the precision of Fig. 3 (b) significantly. On the other hand, the EEMS model improves the sensitivity of Fig. 3 (f) obviously when the similar precision is obtained as TSMS. Therefore, the experiments can demonstrate that as the regularization, Euler's elastica performs better than total variation in removing negligible dots such as noises.

(a) Given image

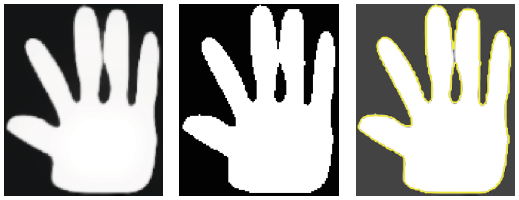

(b) TSMS: g (c) TSMS K-means (d) TSMS contour

(e) Our: g (f) EEMS (g) EEMS contour

Fig. 2. Hand phantom segmentation. The parameters for the model (5) read $a = 10^{-2}$, $b = 2.0$, $\mu = 1.0$, $\eta = 20.0$ while the parameters for ALM are chosen as $r_1 = 5.0$, $r_2 = 20.0$, $r_3 = 5.0$.

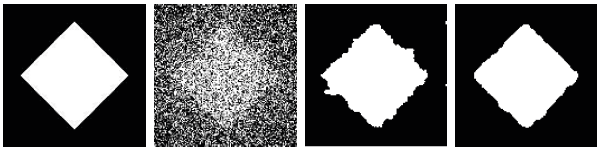

(a) Ground truth (b) Noisy image (c) TSMS (d) EEMS

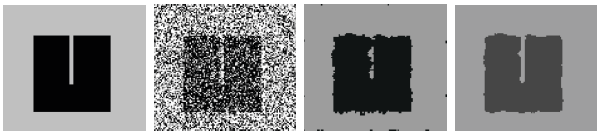

(e) Ground truth (f) Noisy image (g) TSMS (h) EEMS

Fig. 3. Noisy image segmentation. The parameters for the model (5) read $a = 10^{-2}$, $b = 4.0$, $\mu = 1.0$, $\eta = 1.0$ for both test images while the parameters for ALM are chosen as $r_1 = 1.5$, $r_2 = 8.0$, $r_3 = 2.5$ and $r_1 = 0.5$, $r_2 = 2.0$, $r_3 = 0.5$ for (a) and (f), respectively.

B. Tubular images with intensity inhomogeneity

Example 4: Vessel images. We apply the proposed models to medical images with tubular vessels in inhomogeneous backgrounds. The vessels in the given image in Fig. 4 (a) have elongated structures and are in an inhomogeneous background. Firstly, we look at the solution g in the first stage of TSMS and EEMS model, which are displayed Fig. 4 (b) and (d), respectively. We can observe that the vascular structures in Fig. 4 (d) seem more distinguishable than Fig. 4 (b), which is also demonstrated by the K-means results in Fig. 4 (c) and (e), respectively. Therefore, it shows that Euler's elastica makes the

Mumford-Shah functional able to locate meaningful elongated vessels while prohibiting disproportionate fine details or noise. However, the branches of the vessel from the K-means in Fig. 4 (e) seems thin and weak. Thus, we implement the bias-corrected FCM to eliminate the effect of inhomogeneity in the solution g and better segmentation result is obtained as shown in Fig. 4 (f).

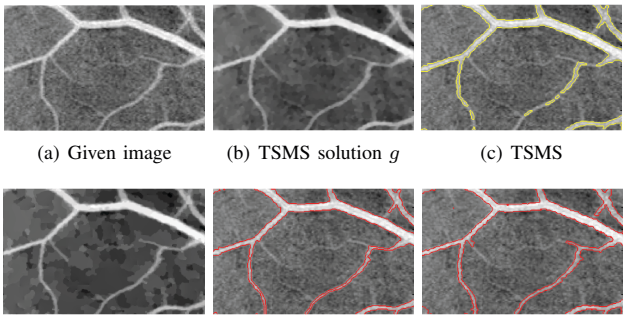

(a) Given image (b) TSMS solution g (c) TSMS

(d) Our solution g (e) EEMS (f) BCEEMS

Fig. 4. Tubular vessels segmentation. The parameters for the model (5) read $a = 10^{-3}$, $b = 1.0$, $\mu = 1.0$, $\eta = 10.0$ while the parameters for ALM are chosen as $r_1 = 3.0$, $r_2 = 8.0$, $r_3 = 1.0$.

For vessel images in Fig. 5 (a) and Fig. 6 (a), some parts of the vessel boundaries are quite weak. Although both the TSMS and the EEMS model fail to segment the complete vessel structures based on K-means clustering as shown in Fig. 5 (c), (e) and Fig. 6 (c), (e), respectively, the EEMS model gives the better results than the TSMS model. In this case, we further apply the bias-corrected FCM to the smooth solution g of EEMS shown in 5 (d) and fig. 6 (d). As shown in Fig. 5 (f) and Fig. 6 (f), the BCEEMS model archives satisfactory segmentation results for such images with intensity inhomogeneity.

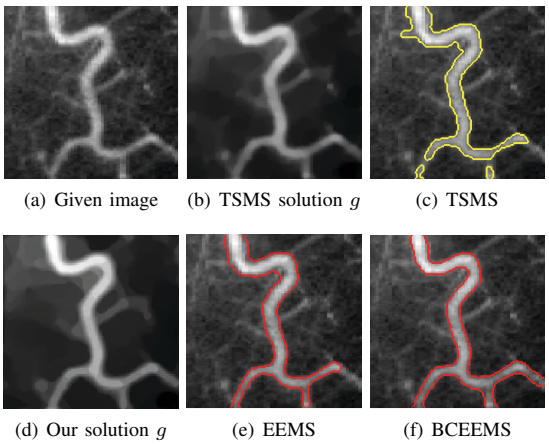

(a) Given image (b) TSMS solution g (c) TSMS

(d) Our solution g (e) EEMS (f) BCEEMS

Fig. 5. Tubular vessels segmentation. The parameters for the model (5) read $a = 10^{-3}$, $b = 3.0$, $\mu = 1.0$, $\eta = 1.0$ while the parameters for ALM are chosen as $r_1 = 0.08$, $r_2 = 1.0$, $r_3 = 1.0$.

C. Multi-phase Segmentation

Example 5: CT angiography image. We begin the multi-phase segmentation with a 2D maximum intensity projection

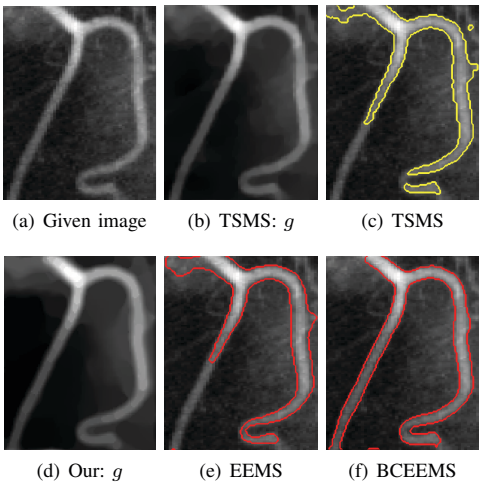

(a) Given image (b) TSMS: g (c) TSMS

(d) Our: g (e) EEMS (f) BCEEMS

Fig. 6. Tubular vessels segmentation. The parameters for the model (5) read $a = 10^{-3}$, $b = 2.0$, $\mu = 2.0$, $\eta = 1.0$ while the parameters for ALM are chosen as $r_1 = 0.1$, $r_2 = 2.0$, $r_3 = 0.5$.

(MIP) image of a 3D CT angiography data in Fig. 7 (a). We applied the three-phase segmentation models to extract the vascular structures from the given MIP image. The segmentation result of the phase (phase 3) containing the aorta and a branch of coronary artery from the TSMS, EEMS, BCEEMS model are displayed in Fig. 7 (b), (c) and (d), respectively. We observe that as the regularization, Euler's elastica can identify some finer details of peripheral vessels compared to TSMS and the bias-corrected FCM can remove the effect of the intensity inhomogeneity.

(a) Given image (b) TSMS (c) EEMS (d) BCEEMS

Fig. 7. Tubular vessels segmentation. The parameters for the model (5) read $a = 10^{-3}$, $b = 2.0$, $\mu = 0.5$, $\eta = 25.0$ while the parameters for ALM are chosen as $r_1 = 5.0$, $r_2 = 15.0$, $r_3 = 5.0$.

Example 6: Brain MRI image. Intensity inhomogeneity is also typical in MR images. There are three tissue classes in MR images: cerebrospinal fluid, gray matter and white matter. Thus, we implemented the four-phase segmentation models on a brain MR image in Fig. 8 (a) with noise 7% and the intensity non-uniformity (INU) 20%, which is from McGill Brain Web, "http://www.bic.mni.mcgill.ca/brainweb/". The segmentation results of each phase obtained by TSMS, EEMS and BCEEMS are shown in the second, third and fourth row of Fig. 8, respectively. Correspondingly, we also display the ground truth of each phase for the given MR image in the last row of Fig. 8. From the figure, we can see that more

details are segmented correctly using the proposed EEMS and BCEEMS model. Furthermore, we compute both the precision and sensitivity of the segmentation results in Table II for the quantitative evaluation. Both precision and recall agree with our hypothesis that Euler's elastica can improve the segmentation, especially when bias is eliminated by bias-corrected FCM.

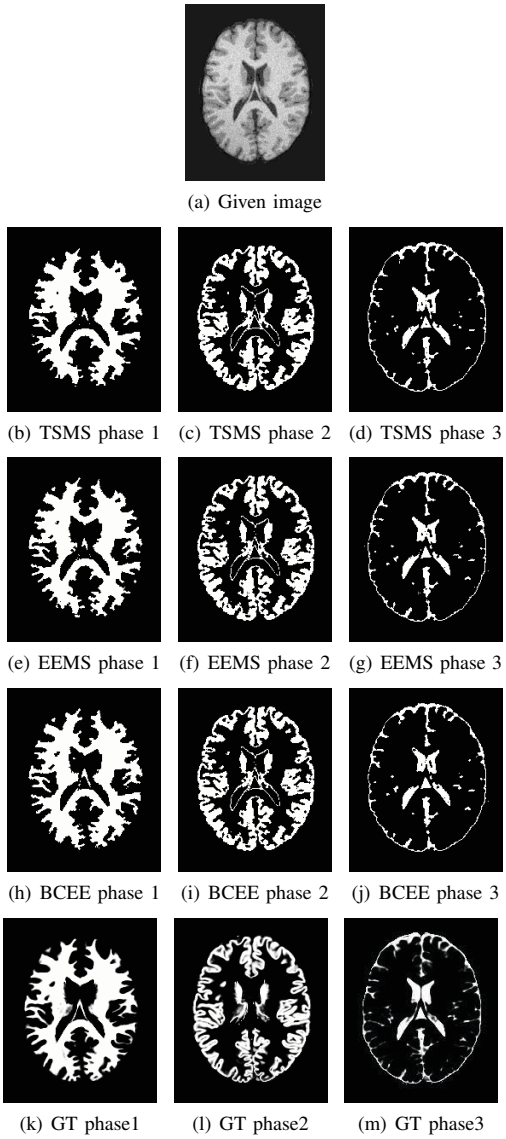

(a) Given image

(b) TSMS phase 1 (c) TSMS phase 2 (d) TSMS phase 3

(e) EEMS phase 1 (f) EEMS phase 2 (g) EEMS phase 3

(h) BCEE phase 1 (i) BCEE phase 2 (j) BCEE phase 3

(k) GT phase1 (l) GT phase2 (m) GT phase3

Fig. 8. Brain MRI segmentation. The parameters for the model (5) read $a = 10^{-3}$, $b = 1.0$, $\mu = 0.5$, $\eta = 15.0$ while the parameters for ALM are chosen as $r_1 = 0.08$, $r_2 = 1.0$, $r_3 = 0.1$. GT denotes Ground Truth.

TABLE II. PRECISION AND SENSITIVITY OF BRAIN EXPERIMENT.

	Phase 1		Phase 2		Phase 3	
	PRE	SEN	PRE	SEN	PRE	SEN
TSMS	0.9515	0.9207	0.8531	0.8858	0.7976	0.8208
EEMS	0.9516	0.9212	0.8543	0.8858	0.7974	0.8315
BCEEMS	0.9412	0.9534	0.8906	0.8734	0.8034	0.8356

V. CONCLUSION

In this paper, we proposed an approach to image segmentation that uses Euler's elastica as the regularization to the Mumford-Shah functional. The two-stage segmentation framework was applied to solve the Euler's elastica regularized Mumford-Shah model. In the first stage, we computed a smooth solution of the variant Mumford-Shah model by augmented Lagrangian method while in the second stage, the K-means clustering was implemented to threshold the solution into different regions. Compared to the Mumford-Shah model relied on the total length regularization, Euler's elastica has good properties in interpolating missing parts and capturing fine elongated structures, which are useful for fine medical image structure segmentation. In addition, we address the intensity inhomogeneity widely existing in medical imaging by the bias-corrected FCM. Shown in the experiments, the proposed model outperforms the TSMS model [5] in both image segmentation and denoising applications. Different kinds of applications, such as tubular and irregular shaped, CTA and MR images in different noise levels, are tested to demonstrate the performance of the proposed model.

ACKNOWLEDGMENT

The work is partially supported by A*STAR BEP Grant 132 148 0008, Singapore. The second author Dr. Chang Huibin is supported by PHD Programme 52XB1304 of Tianjin Normal University.

REFERENCES

[1] D. Mumford and J. Shah, "Optimal approximations by piecewise smooth functions and associated variational problems," *Communications on pure and applied mathematics*, vol. 42, no. 5, pp. 577–685, 1989.

[2] T. F. Chan and L. A. Vese, "Active contours without edges," *IEEE Transactions on Image Processing*, vol. 10, no. 2, pp. 266–277, 2001.

[3] L. A. Vese and T. F. Chan, "A multiphase level set framework for image segmentation using the mumford and shah model," *International journal of computer vision*, vol. 50, no. 3, pp. 271–293, 2002.

[4] A. Tsai, A. Yezzi Jr, and A. S. Willsky, "Curve evolution implementation of the mumford-shah functional for image segmentation, denoising, interpolation, and magnification," *IEEE Transactions on Image Processing*, vol. 10, no. 8, pp. 1169–1186, 2001.

[5] X. Cai, R. Chan, and T. Zeng, "A two-stage image segmentation method using a convex variant of the mumford–shah model and thresholding," *SIAM Journal on Imaging Sciences*, vol. 6, no. 1, pp. 368–390, 2013.

[6] D. Mumford, "Elastica and computer vision," *Algebriac Geometry and Its Applications*, pp. 491–506, 1994.

[7] W. Zhu, X.-C. Tai, and T. Chan, "Image segmentation using eulers elastica as the regularization," *Journal of Scientific Computing*, vol. 57, no. 2, pp. 414–438, 2013.

[8] J. Shen, S. H. Kang, and T. F. Chan, "Euler's elastica and curvature-based inpainting," *SIAM Journal on Applied Mathematics*, vol. 63, no. 2, pp. 564–592, 2003.

[9] S. Esedoglu and J. Shen, "Digital inpainting based on the mumford–shah–euler image model," *European Journal of Applied Mathematics*, vol. 13, no. 04, pp. 353–370, 2002.

[10] E. Bae, J. Shi, and X.-C. Tai, "Graph cuts for curvature based image denoising," *IEEE Transactions on Image Processing*, vol. 20, no. 5, pp. 1199–1210, 2011.

[11] X.-C. Tai, J. Hahn, and G. J. Chung, "A fast algorithm for euler's elastica model using augmented lagrangian method," *SIAM Journal on Imaging Sciences*, vol. 4, no. 1, pp. 313–344, 2011.

[12] C. Wu, X.-C. Tai *et al.*, "Augmented lagrangian method, dual methods, and split bregman iteration for rof, vectorial tv, and high order models." *SIAM Journal on Imaging Sciences*, vol. 3, no. 3, pp. 300–339, 2010.

[13] J. A. Hartigan and M. A. Wong, "A k-means clustering algorithm," *Journal of the Royal Statistical Society. Series C (Applied Statistics)*, vol. 28, no. 1, pp. 100–108, 1979.

[14] M. N. Ahmed, S. M. Yamany, N. Mohamed, A. A. Farag, and T. Moriarty, "A modified fuzzy c-means algorithm for bias field estimation and segmentation of mri data," *IEEE Transactions on Medical Imaging*, vol. 21, no. 3, pp. 193–199, 2002.

[15] L. C. Evans, "Partial differential equations," *American mathematical society*, 1998.